J. Biochem. **138**, 413–423 (2005)
doi:10.1093/jb/mvi142

Possible Role of Each Repeat Structure of the Microtubule-Binding Domain of the Tau Protein in *In Vitro* Aggregation

Koji Tomoo[1,*], Tian-Ming Yao[2,*], Katsuhiko Minoura[1], Shuko Hiraoka[1], Miho Sumida[3], Taizo Taniguchi[3] and Toshimasa Ishida[1]

[1]Osaka University of Pharmaceutical Sciences, 4-20-1 Nasahara, Takatsuki, Osaka 569-1094; [2]Department of Chemistry, Tongji University, Shanghai 200092, P.R. China and [3]Behavioral and Medical Sciences Research Consortium, 2-5-7 Tamachi, Akashi, Hyogo 673-0025

Received April 20, 2005; accepted July 15, 2005

Although one of the priorities in Alzheimer's research is to clarify the filament formation mechanism of the tau protein, it is currently unclear how it is transformed from a normal structure in a neuron. To examine which part and what structural change in the tau protein are involved in its transformation into a pathological entity, the initial *in vitro* self-aggregation features of each repeat peptide (R1–R4) constituting a three- or four-repeat microtubule-binding domain (3RMBD or 4RMBD) in the tau protein was investigated by measuring both the fluorescence and light scattering (LS) spectra on the same instrument, because these MBD domains constitute the core moiety of the tau paired helical filament (PHF) structure. The conformational features of the R1 and R4 peptides in trifluoroethanol were also investigated by ^{1}H-NMR and molecular modeling analyses and compared with those of the R2 and R3 peptides. The analyses of the LS spectra clarified (i) the self-aggregation rates of R1–R4, 3RMBD and 4RMBD at a fixed concentration (15 mM), (ii) their minimum concentrations for starting filament extension, and (iii) the concentration dependence of their self-aggregations. The fluorescence analyses showed that the R2 and R3 peptides have high self-aggregation abilities at the extension and nucleation steps, respectively, in their filament formation processes. It was shown that the R2 repeat exhibits a positive synergistic effect on the aggregation of 4RMBD. The R1 and R4 repeats, despite their weak self-aggregation abilities, are necessary for the intact PHF formation of tau MBD, whereas they exerted a negative effect on the R3-driven aggregation of 3RMBD. The conformational analyses showed the importance of the amphipathic conformational features of the R1 to R4 peptides, and the intermolecular disulfide bonding abilities of the R2 and R3 peptides for the PHF formation. On the basis of the present spectral and conformational results, the possible role of each repeat structure in the dimeric formation of MBD at the initial *in vitro* aggregation stage is discussed.

Key words: aggregation, fluorescence, light scattering, microtubule-binding domain, repeat structure, solution conformation, tau protein.

Abbreviations: 3RMBD, three-repeat microtubule-binding domain; 4RMBD, four-repeat microtubule-binding domain; AD, Alzheimer's disease; CD, circular dichroism; DQF-COSY, double quantum-filtered chemical shift-correlated spectroscopy; DTT, dithiothreitol; EM, electron microscopy; FTDP-17, frontotemporal dementia with parkinsonism linked to chromosome 17; HPLC, high-pressure liquid chromatography; I_{LS}, intensity of light scattering; LS, light scattering; LLS, laser light scattering; MBD, microtubule-binding domain; MAP, microtubule-binding protein; MT, microtubule; NOE, nuclear Overhauser effect; NOESY, nuclear Overhauser effect spectroscopy; PHF, paired helical filament; R1, first repeat peptide of the four-repeat microtubule-binding domain; R2, second repeat peptide of the four-repeat microtubule-binding domain; R3, third repeat peptide of the four-repeat microtubule-binding domain; R4, fourth repeat peptide of the four-repeat microtubule-binding domain; RMSD, root-mean-square deviation; SA, simulated annealing; SDS-PAGE, sodium dodecylsulfate polyacrylamide gel electrophoresis; TFA, trifluoroacetic acid; TFE, trifluoroethanol; ThS, thioflavin S; TOCSY, total correlation spectroscopy; TSP, 3-(trimethylsilyl)propionic acid.

Microtubules (MTs) play an important role in the maintenance of cell shape, cell division, axonal transport, secretion, and receptor activity, and maintain their functions with the help of microtubule-associated proteins (MAPs) (*1*). Tau protein, one of the neuronal MAPs in the mammalian brain, included six isoforms from 352 to 441 amino acids in length, and these isoforms are produced from a single human tau gene by alternative mRNA splicing of exons 2, 3 and 10 located on chromosome 17 (*2–5*). The MT-binding region of the tau protein is located in the C-terminal half and is called the microtubule-binding domain (MBD) (*6*, *7*). It is composed of a three- or four-repeat structure (3RMBD or 4RMBD, respectively), where each repeat peptide (named R1 to R4, from the first unit to the fourth unit) consists of 31 or 32 amino acid residues (Fig. 1). No notable dissimilarity is observed

*To whom correspondence should be addressed. Fax: +81-72-690-1068, E-mail: tomoo@gly.oups.ac.jp or tmyao@mail.tongji.edu.cn

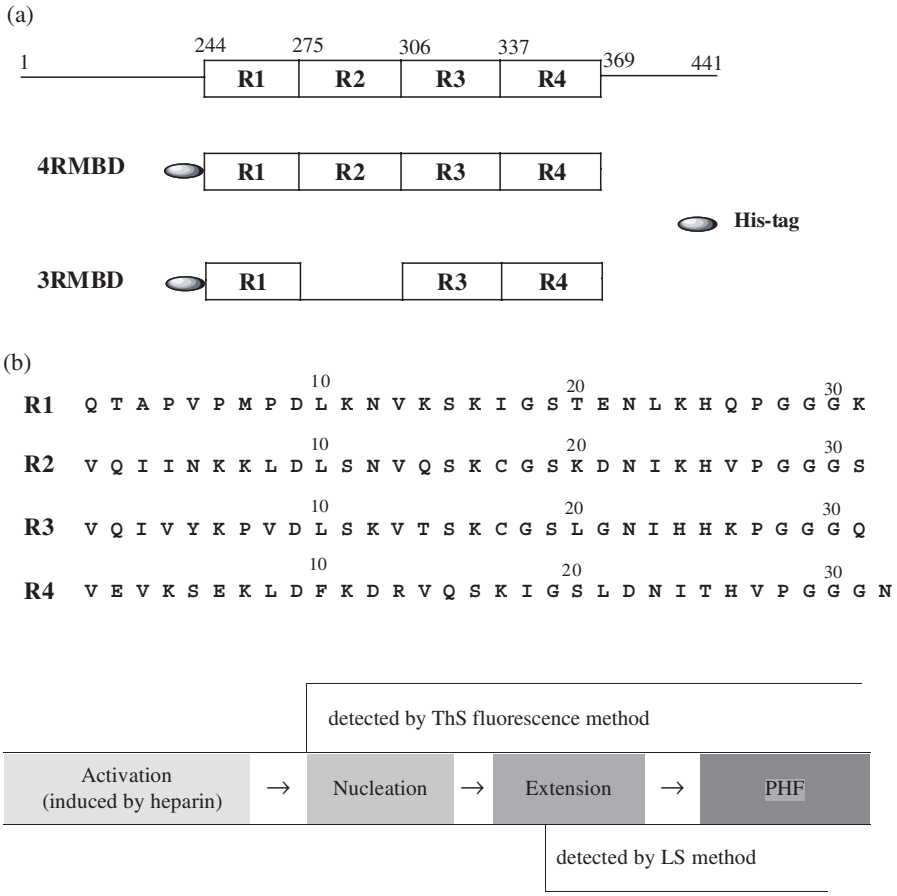

Fig. 1. **(a) Schematic diagram of the entire four-repeat human tau protein, His-tagged four-repeat MBD (4RMBD) and three-repeat MBD (3RMBD) used in this work, and (b) the amino acid sequences of these repeat peptides.** The regions from the first to the fourth repeat structure in MBD are named R1 to R4, respectively. The number of amino acid residues in (a) refers to the longest isoform of the human tau protein (441 residues).

Fig. 2. **Schematic representation of the filament accumulation process of the tau repeat peptide or MBD, monitored by light scattering and ThS fluorescence assays.**

among the four repeat structures, and they have relatively similar and conserved amino acid sequences.

The tau protein is by nature a highly soluble protein with a random conformation in aqueous solution, and shows hardly any tendency to assemble under physiological conditions. In the brains of Alzheimer's disease (AD) patients, however, it dissociates from axonal MTs and aggregates abnormally to form an insoluble paired helical filament (PHF), which is implicated in neurodegeneration (*2*). Therefore, one of the priorities in Alzheimer research is to elucidate the mechanism of PHF formation by the tau protein, because such knowledge could potentially lead to the development of therapeutic strategies. However, a definite conclusion has not yet been drawn because of the lack of PHF structural information at the atomic level, although many *in vivo* and *in vitro* studies have been performed thus far (*8–11*).

As a useful approach to achieving this end, it appears important to clarify which part and what structural change in the tau protein are most responsible for its transformation into a PHF. Since the MBD repeat structure constitutes the core moiety of the PHF structure (*6*, *12*), and many mutations in FTDP-17 lie in MBD (*2*, *13*), analysis of the self-assembly of each repeat peptide is important to clarify the mechanism of MBD filament formation, even though the filament of each repeat peptide may not directly reveal the intact features of the tau PHF structure. Therefore, we have been investigating the conformational and self-associational features of each repeat peptide in MBD by various spectroscopic methods (*14–18*), because such data are minimally available at present.

To monitor the *in vitro* aggregation of the tau protein, several different techniques have been employed. A widely used method for assessing the polymerization of filamentous macromolecular compounds is the light scattering (LS) method, which measures the turbidity of the reaction solution (*19*). In this method, the laser light scattering (LLS) method has usually been used to increase the sensitivity of monitoring the polymerization of tau *in vitro* (*20*). However, we have succeeded for the first time in monitoring tau aggregation under physiological conditions (around 4 μM) by the 90° angle light scattering (LS) method, in which the sensitivity of LS is increased by carefully selecting the wavelength of the incident light and applying 90° angle light scattering. Compared with the LLS method, the LS measurement can be performed directly on the fluorescence instrument, and is, therefore, more convenient to use. On the other hand, it has been reported that the fluorescence measurement of a thioflavin dye such as ThS (thioflavin S) can be used to monitor filament formation in solution in real time (*21*).

The process of self-aggregation of the tau peptide can be divided into the following steps: activation → nucleation → extension → PHF (Fig. 2). Although both the ThS fluorescence and LS methods can be used to monitor aggregation, their principles are different, *i.e.*, the LS method is only sensitive to insoluble filament formation *via* the extension step in solution (*19*, *20*, *22*), whereas the ThS fluorescence

method can also cover the nucleation step before the extension step (*21*, *23*). Thus, a detailed analysis of the whole self-aggregation process (nucleation → elongation → PHF formation) of the tau peptide can be expected by using a combination of these two methods.

To evaluate the contribution of each repeat structure to MBD filament formation quantitatively, we investigated the *in vitro* aggregation features of four repeat peptides by a combination of the ThS fluorescence and LS methods. Also, the conformations of R1 and R4 in trifluoroethanol (TFE) solution were determined by CD, ^{1}H-NMR and molecular modeling analyses, and compared with those of R2 and R3 (*15*, *16*) to consider the conformational contribution of each repeat peptide to the self-aggregation of MBD. In this paper, we report our results and discuss the possible role of each repeat structure in the initial *in vitro* aggregation of MBD.

MATERIALS AND METHODS

Chemicals and Recombinant MBDs—Heparin (average molecular weight, 6000) and thioflavin S (ThS) were obtained from Sigma Co. Tau repeat peptides (R1, R2, R3, and R4) were chemically synthesized using a solid-phase peptide synthesizer. These peptides were characterized by mass spectrometry and determined to be >95.0% pure by reverse-phase HPLC. The samples (including TFA as a counterion) were obtained in the lyophilized form. The gene expression and purification of His-tagged three- and four-repeat MBDs (3RMBD and 4RMBD) of human brain tau (Fig. 1) were performed according to a previous paper (*11*). Their purities were confirmed by SDS-PAGE analyses.

Light Scattering Assay of Aggregation—Insoluble filament formation via the extension processes of each repeat peptide was measured by 90° angle light scattering (LS) using a JASCO spectrofluorometer (model FP6500), where the excitation and emission wavelengths were both set at 550 nm. The peptide was adjusted to a final concentration of 15 μM in 50 mM Tris-HCl buffer (pH 7.5) and placed in a fluorometer cuvette with a 1-cm pathlength. The sample (~300 μl) was maintained at 37°C by a circulating water bath, and heparin was added to achieve a final reaction concentration of 3.8 μM. The intensity change of LS after heparin addition was plotted as a function of time. Although data were collected every 2 s, we used only data obtained every 30 s or 1 min, and in some instances, 2 min for the purposes of plotting.

On the other hand, the concentration dependence of LS intensity was determined as follows. Repeat peptides of various concentrations (3–25 μM) were prepared in 50 mM Tris-HCl buffer (pH 7.5). After adding heparin to a final concentration of 3.8 μM, the peptides were incubated at 37°C overnight. Then, their LS intensities at 550 nm were measured as a function of concentration. All experiments were performed at least three times, and the data were averaged.

ThS Fluorescence Assay of Aggregation—The concentration of each repeat peptide was adjusted to 15 μM using 50 mM Tris-HCl buffer (pH 7.5) containing 10 μM ThS dye. After adding heparin to a final concentration of 3.8 μM, the time-dependent change in fluorescence intensity at 37°C was monitored on a JASCO FP6500 instrument with a 2-mm quartz cell with excitation at 440 nm and emission at 490 nm. The background fluorescence of the sample was subtracted when needed.

For the seeding experiment, seeds were prepared by incubating 15 μM peptide mixed with 3.8 μM heparin in 50 mM Tris-HCl buffer (pH 7.5) at 37°C overnight. The filaments formed were then ultrasonicated with an ultrasonic disrupter (UD200, Tomy Seiko Co.) for 3–4 min.

CD Measurement—The sample solution was adjusted to 40 μM in water, TFE, and a mixture of these solvents, with the pH was adjusted to 7.5 by the addition of HCl or NaOH. All measurements were carried out at 25°C with a JASCO J-820 spectrometer in a cuvette with a 2-mm path length. For each experiment, the measurement from 190 nm to 260 nm was repeated eight times under N_2 gas flow, and the results were summed. Then, the molar ellipticity was determined after normalizing the sample concentration. The same experiment was performed at least three times using the newly prepared samples, and average values are presented in this paper. Data are expressed as mean residue ellipticity [θ] in units of deg cm^2 dmol^{-1}.

^{1}H-NMR Measurement and 3D Molecular Modeling of R1 and R4 Peptides—The methods for proton peak assignment and 3D molecular construction were the same as those used for R2 and R3 (*15*, *16*). The ^{1}H-NMR spectra of the peptides (2 mM) dissolved in TFE-d_2 were recorded with a Varian Unity INOVA500 spectrometer. ^{1}H chemical shifts were referenced to 0 ppm for TSP at 298 K. Because of the low solubility at pH > 5.0, the pH was adjusted to 3.9 with HCl or NaOH. In order to trace direct single- and multiple-relayed through-bond connectivities successively, TOCSY spectra were recorded at mixing times of 40 and 100 ms. The NOESY spectra were also measured at mixing times of 100, 200, and 300 ms. Assuming the same correlation time for all protons, the offset dependence of the NOESY cross peaks was used to estimate proton-proton distance. The vicinal coupling constants obtained from DQF-COSY measurements were used to estimate the possible torsion angles: $^3J_{\mathrm{HN}C\alpha\mathrm{H}} = 1.9–1.4\cos\theta + 6.4\cos^2\theta$, where $\phi = |\theta - 60|^\circ$ for the φ torsion angle around the C'_{i-1}-N_i-$C\alpha_i$-C'_i bond sequence (*24*).

Three-dimensional structures that fulfill the NOE distance and *J* torsion angle constraints of intramolecular proton pairs were constructed by dynamic SA calculations (*25*) using the CNS program (*26*). After randomization of the peptide into extended strands corresponding to each disjointed molecular entity, the initial structures were constructed by referring to NMR data structures and statistical analysis of the averaged properties of many peptides. The constructed structures were then annealed for 15 ps at 50,000 K and cooled to 300 K at a rate of 250 K/step for 10 ps, and the minimization of more than 5,000 steps was continued. The constraints for distances and torsion angles were used as harmonic potential functions. As the input data for the distance constraint, the proton-proton pairs were classified into three distance groups according to their NOE intensities: strong (1.8–3.0 Å), medium (1.8–4.0 Å) and weak (1.8–5.0 Å). The torsional constraint was applied to the φ torsion angle, that is, –120 ± 40° for $^3J_{\mathrm{HN}C\alpha\mathrm{H}} > 8$ Hz, –75 ± 25° for $^3J_{\mathrm{HN}C\alpha\mathrm{H}} < 6$ Hz, and –100 ± 60° for the others. The

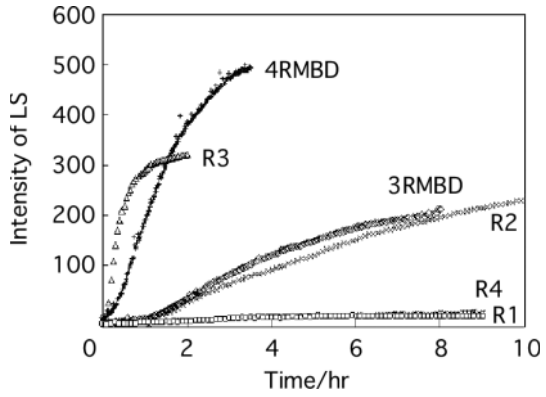

Fig. 3. **Time dependence of LS intensities of tau repeat peptides**. The intensity of the 90° angle LS of each repeat peptide (15 μM concentration in 50 mM Tris-HCl buffer, pH 7.5) was monitored as a function of time (h) at 37°C after the addition of 3.8 μM heparin, with the excitation and emission wavelengths both set at 550 nm.

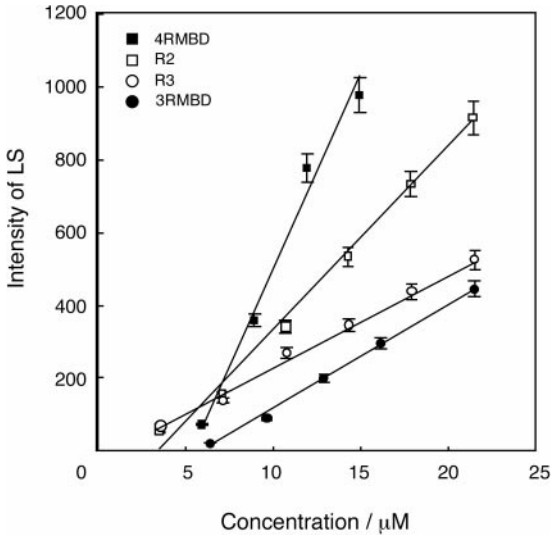

Fig. 4. **Concentration dependence of LS intensities for R2 (open squares), R3 (open circles), 3RMBD (filled circles) and 4RMBD (filled squares)**. Each repeat peptide was prepared using 50 mM Tris-HCl buffer (pH 7.5). After adding 3.8 μM heparin, the peptide was incubated at 37°C overnight. The intensity of LS (I_{LS}) was plotted as a function of concentration, with the excitation and emission wavelengths both set at 550 nm. The observed intensities were fitted to straight lines with $r > 0.98$ by linear regression.

RMSD analyses of the energy-minimized structures were carried out using the MOLMOL program (*27*).

RESULTS

Aggregation Kinetics of Repeat Peptides by Light Scattering—The 90° angle LS measurement is a useful method for directly assessing the aggregation process of tau protein. Since ideal Rayleigh scattering is dependent on the radius of the particles, the wavelength for monitoring the aggregates of the tau repeat peptides was surveyed by synchronous scanning with a fluorometer, and the excitation and emission wavelengths of 550 nm were found to be most suitable for the dimensions of the filaments of R2, R3, 3RMBD and 4RMBD.

The intensity–time profiles of repeat peptides at fixed concentration (15 μM) are shown in Fig. 3. These results indicate that the aggregation rates of these repeat peptides are totally different from one another. The R3 peptide accumulated most quickly, with a half time of 0.5 ± 0.1 h. The R2 peptide accumulated much more slowly than R3 (half time = 15 ± 3 h), although the LS intensity of the 15 μM R2 peptide after standing overnight was larger than that of R3 (see Fig. 4). In contrast, no apparent increase in LS intensity was observed for the R1 and R4 peptides within this experimental time, indicating that their self-aggregation abilities are very weak compared with those of R2 and R3. On the other hand, the aggregation profiles of 4RMBD and 3RMBD also differed considerably from each other. It was seen that 4RMBD accumulated faster (half time = ~1.0 h) than 3RMBD (half time > 3.0 h). Since the absence/presence of the R2 repeat differentiates the 4RMBD/3RMBD structures, this accumulation difference may indicate that the R2 repeat structure plays an important role in promoting the aggregation of the tau MBD region.

Critical Concentration of the Repeat Structure for Filament Formation—The repeat peptides at various concentrations were incubated overnight at 37°C in 50 mM Tris-HCl buffer containing 3.8 μM heparin, and their LS intensities were measured. The intensity–concentration profiles are shown in Fig. 4, and the *x*-intercepts and slopes of the respective regression lines are given in Fig. 5. The respective profiles were fitted to the straight lines of $r^2 \geqslant 0.98$ by linear regression analysis in the concentration ranges of 4–21 μM for R2, 4–21 μM for R3, 7–21 μM for 3RMBD, and 5–15 μM for 4RMBD; reliable data were not obtained for concentrations above about 25 μM because of precipitation of the filaments in the solution.

tau construct	slope	x-intercept (critical conc., μM)
R1	0	—
R2	49.8 ± 1.3	3.40 ± 0.18
R3	25.7 ± 0.9	1.05 ± 0.21
R4	0	—
3RMBD	28.7 ± 0.9	6.06 ± 0.07
4RMBD wild	104.4 ± 1.6	5.26 ± 0.10

Fig. 5. **Slopes and *x*-intercepts of repeat peptides, 3RMBD and 4RMBD**. The values are the averages of three trials.

The *x*-intercepts in Fig. 5 indicate the critical concentrations of the respective MBD constructs for starting the filament extension process within the sensitivity of the LS method (see Fig. 2). These data reflect the thermodynamic features of filament formation, obtained by steady state experiments (measurement at an equilibrium state after overnight incubation). The value of the critical concentration demonstrates the ease with which the tau

peptide forms insoluble filaments. No tau peptide can effectively form mature filaments (*via* the extension process) at concentrations below the critical concentration. Peptides with small x-intercepts can start the extension reaction in more dilute solutions (at lower concentrations), and vice versa. It should be noted that these data are incommensurable with the LS intensity–time profile in Fig. 3, because the latter illustrates the speed of filament growth at a fixed concentration (15 μM) of repeat peptide (a dynamic feature). Additionally, the critical concentration did not necessarily correlate with the association rate obtained by the ThS fluorescence method (*11*, *16*, *17*), the dynamic feature of filament formation including the nucleation process of the tau repeat peptide in the solution state (discussed later).

Comparison of the ThS Fluorescence and LS Methods for Aggregation of a Repeat Peptide—As stated in the Introduction, the nucleation → extension → PHF formation process for filament formation could be monitored by a combination of the ThS fluorescence and LS methods. The time–intensity profiles of the R2 and R3 peptides are shown in Fig. 6, in which the fluorescence and LS intensities are plotted on the same time scale, on the basis of the intensities of both profiles saturated at 120 min in the case of the R3 peptide. Although the two curves for LS (broken line) and ThS fluorescence (solid line) show similar sigmoidal-like profiles, the characteristic difference in peptides could be observed in their filament formation processes.

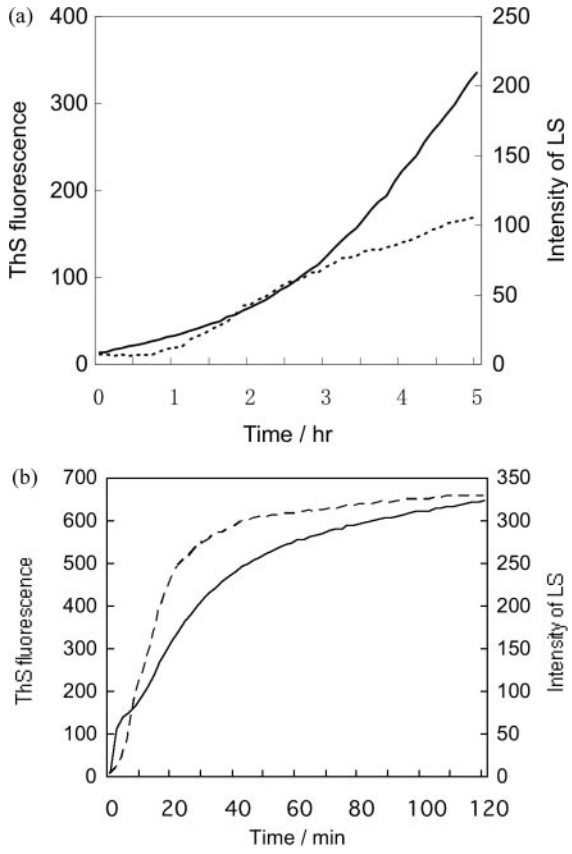

Fig. 6. **Time profiles of ThS fluorescence (solid lines) and LS (broken lines) intensities of the (a) R2 and (b) R3 peptides**. The ThS fluorescence and LS intensities of 15 μM R2 and R3 peptides (50 mM Tris-HCl buffer, pH 7.5) were monitored as functions of time at 37°C after the addition of 3.8 μM heparin, with the excitation and emission wavelengths both set at 550 nm for LS and at 440 nm and 550 nm for ThS measurement.

Concerning the R3 peptide (Fig. 6b), the LS intensity showed a lag time of about 3 min after the addition of heparin, while the ThS fluorescence intensity increased abruptly without any lag phase. Then, at about 7 min, the ThS fluorescence curve was preceded by the LS curve. After that, both the LS and fluorescence curves reached a plateau in almost the same time range from about 40 min to 120 min. Since the ThS fluorescence and LS methods can monitor the processes from the nucleation step and extension step, respectively (Fig. 2), these different profiles show that filament formation of the R3 peptide is mainly a fast nucleation process, where the initial reaction time up to ~7 min (especially in first 3 min, the LS curve shows a lag phase, while the ThS fluorescence shows an abrupt increase) may be spent in forming the nucleation core, which is more sensitive to ThS fluorescence than to LS.

In contrast, the R2 peptide aggregated very slowly. As shown in Fig. 6a, the overall rates of increase of both intensities were relatively small, and the ThS fluorescence curve was mostly ahead of the LS curve. At the beginning of the reaction, both the LS and ThS fluorescence intensities increased very slowly. This time–intensity profile suggests that filament formation of the R2 peptide proceeds with a slow nucleation process, consistent with the results of the seeding effect of R2 aggregation.

Seeding Effect for the Aggregation of the R2 Peptide—Previously, we investigated the seeding effect of the tau repeat peptide on filament formation and observed that filament formation by the R2 peptide is largely promoted only by a template of homogeneous aggregates, whereas that of the R3 peptide is scarcely affected by any repeat seed. Thus, in order to analyze the R2-dependent seeding effect of the R2 peptide in more detail, the rate of increase in ThS fluorescence intensity was examined as a function of R2 seed concentration. These results are shown in Fig. 7a, and the relationship between the rate of increase in ThS fluorescence intensity and seed concentration is shown in Fig. 7b. Because the nucleation step is skipped in this seeding experiment, the result reflects the extension process of the R2 peptide.

The linear equation of Fig. 7b can be theoretically expressed by

$$\frac{dC}{dt} = k_{on}[M][P - P_0] - k_{off}[P - P_0],$$

where $\frac{dC}{dt}$ = initial velocity of the extension reaction, $[M]$ = initial monomer concentration, $[P]$ = initial seed concentration, P_0 = minimum seed concentration necessary to start the seeding reaction, and k_{on} and k_{off} are the association and dissociation constants of the extension reaction, respectively. However, $k_{on} \gg k_{off}$ should be pointed out for tau aggregation, because no notable dissociation process was observed for pure seeds. Thus, the equation can be simplified as $dC/dt = k_{on}[M][P - P_0]$. The result indicates that the R2 seed-dependent aggregation (filament formation) of the R2 peptide is a first-order reaction, *i.e.*, R2

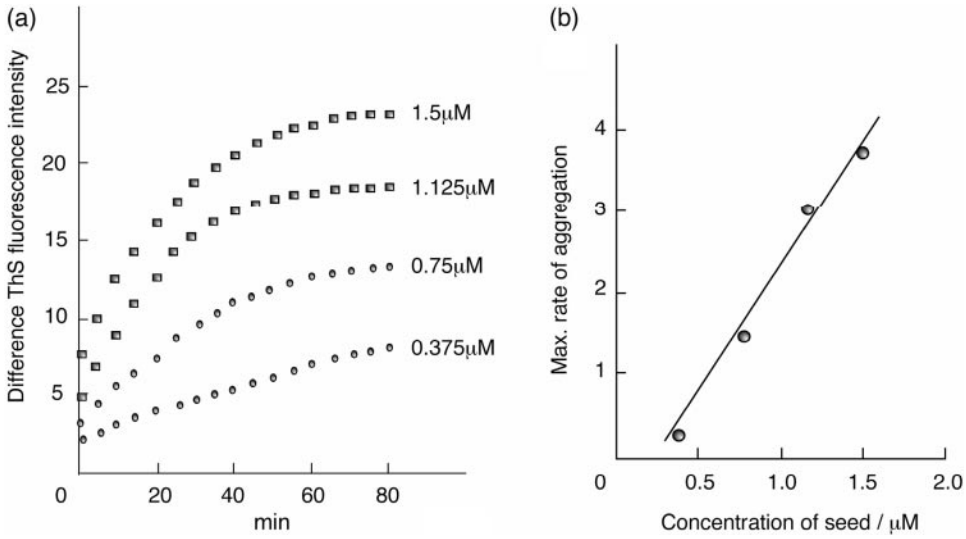

Fig. 7. **Seeding effect on the aggregation of R2 peptide: (a) time dependence of ThS fluorescence intensity at different R2 seed concentration and (b) relation of the maximum aggregation rate to the seed concentration**. R2 peptide (15 μM) was mixed with a small amount of R2 seed (from 0.375 to 1.53 μM) in 50 mM Tris-HCl buffer (pH 7.5), and then 3.8 μM heparin was added to induce aggregation. The aggregation was monitored at 37°C by the ThS fluorescence method, with the excitation and emission wavelengths set at 440 nm and 550 nm, respectively. In (a), the fluorescence intensity of the R2 peptide containing R2 seed was subtracted from that of the R2 peptide without R2 seed. The maximum aggregation rate of (b) corresponds to the steepest slope of each curve in (a).

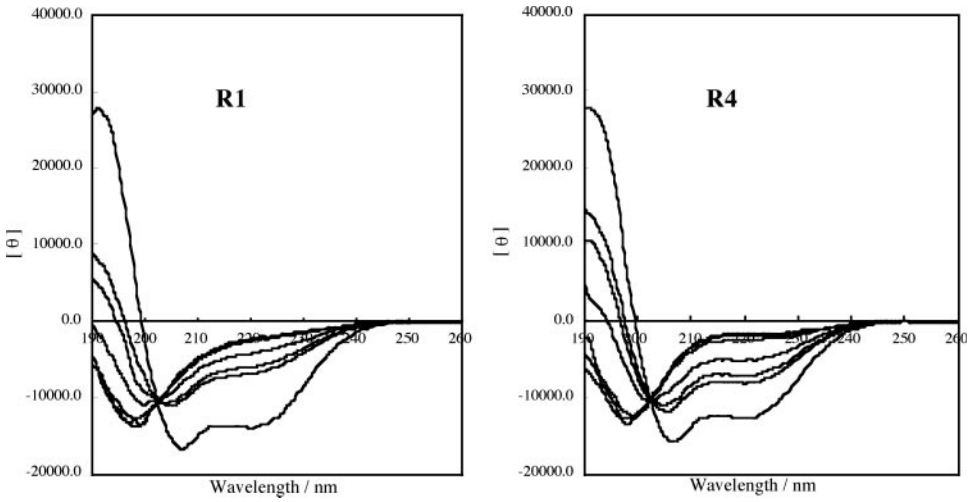

Fig. 8. **CD spectra of R1 and R4 repeat peptides at different water/TFE ratios at pH 4.3**. Curves from top to bottom in the 210–230 nm region were measured spectrally in 0, 5, 10, 20, 30, 50 and 100% TFE. The CD spectra at pH 7.5 were almost the same.

peptide + R2 seed → R2 aggregate, where $k_{on} = (3.2 \pm 0.4) \times 10^6$ M^{-1} min^{-1} and $P_0 = 0.3 \pm 0.1$ μM. The P_0 value is about tenfold smaller than that listed in Fig. 5, indicating a prominent seeding effect for the R2 peptide. However, since such a relationship was not observed in the absence of heparin under the same conditions, it should be noted that the ability of heparin to promote R2-filament formation is much stronger than that of the filamentous R2 template.

TFE-Induced Conformational Changes of Repeat Peptides—To investigate which part of each repeat peptide is most flexible and solvent-sensitive, the CD spectra of the R1–R4 peptides were measured at different water/TFE ratios. The results for R1 and R4 are shown in Fig. 8; those for R2 and R3 were previously reported (*16*). All repeat peptides manifested similar solvent-dependent spectral changes, although the molar ellipticity of R3 was considerably smaller than those of the others. The CD spectra in aqueous solution predominantly show a random conformation characterized by a negative peak at about 197 nm, but the spectra in TFE indicate an α-helical structure characterized by two negative peaks at about 209 nm and 222 nm. The detectable conformational transitions start at approximately 20% TFE, and the α-helical content increases as the TFE content increases and is negligibly affected by the pH change. The conformations reversibly interchanged between the random and helical structures without any notable lag time or energy barrier, depending on the TFE/water ratio. This suggests that all repeat peptides can change their conformations easily, depending on the hydrophobic and hydrophilic balance of the solvent.

On the other hand, the α-helical content calculation (*29*) from the CD ellipticity at 222 nm showed a marked difference in the transition degree to the α-helical structure between R3 and the other peptides; (R1 = 8.1, R2 = 9.7, R3 = 7.6, R4 = 7.0%) at 0% TFE, (10.5, 12.2, 8.0, 10.4%) at 10%, (15.7, 17.6, 12.1, 21.4%) at 20%, (23.3, 21.7, 17.8,

Fig. 9. **Diagram of NOE connectivity between neighboring ($d_{\alpha N(i,i+1)}$, $d_{NN(i,i+1)}$, $d_{\alpha N(i,i+3)}$ and $d_{\alpha\beta(i,i+3)}$) protons of R1 and R4**. The strength of the observed NOE is represented by the thickness of the bar.

29.3%) at 30%, (27.1, 28.2, 20.6, 33.7%) at 50%, and (56.4, 53.6, 34.2, 52.4%) at 100% TFE. This indicates that the TFE content-dependent α-helical region of the R1, R2 or R4 structure is larger than that of R3, indicating that the conformation of the R1, R2 or R4 peptide is more sensitive than that of R3 to changes in external environmental conditions such as the type of solvent.

Conformations of Repeat Peptides in TFE Solution—The R1 and R4 peptide structures in TFE solution were analyzed by both ^{1}H-NMR spectroscopy and molecular modeling calculations, to compare the TFE-induced conformations of the R2 and R3 peptides already determined by the same method (*15*, *16*). The diagram of short-, medium- and long-range proton-proton connectivities along the peptide backbone, observed by NOESY, is shown in Fig. 9. Using NOE constraints for proton-proton distances and $J_{HNC\alpha H}$ constraints for ϕ torsion angles, 100 possible conformers were constructed by dynamic SA calculation. The statistics of the 20 most stable conformers are summarized in Table 1, and their superposition on the backbone structure is shown in Fig. 10. The constructed conformers exhibited the α-helical structures of the Leu10–Lys24 sequence for the R1 peptide and the Ser5–Ser20 sequence for the R4 peptide. Although both the N- and C-terminal moieties were flexible and did not take any definite 3D structure, their extents differed considerably. Large flexibility was observed at the N-terminal region of R1, which is in contrast to the large flexibility at the C-terminal region of R4. Characteristically, both the helical regions of R1 and R4 showed amphipathic residual side chain distributions (Fig. 11). It is noteworthy that the α-helical conformations of the R2 and R3 peptides in the TFE solution take also similar amphipathic residual side chain distributions (*14*, *16*).

Table 1. **Structural statistics for 20 stable structures of R1 and R4 repeat peptides.**

	R1	R4
Number of structures	20	20
Number of constraints		
Total number of NOEs	373	395
Intraresidue NOEs	208	211
Sequential NOEs	103	106
Inter-residue NOEs	62	57
Dihedral angles	20	25
Average value (esd)		
RMS deviation* (backbone) (Å)	0.81(37)	0.68(25)
RMS deviation from NOE (Å)	0.093(1)	0.069(2)
NOE violations > 0.10 Å	10.5(12)	11.0(8)
Energy (kcal/mol)		
Overall	387(7)	315(6)
NOE	182(7)	133(7)
Angle	80(3)	90(3)
Bond	25(1)	25(1)
Improper	20(1)	9.0(8)
van der Waals	79(4)	58(4)

* Calculated from residues 10 to 24 for R1 and residues 5 to 22 for R4.

DISCUSSION

To monitor the *in vitro* aggregation of the tau protein, several different techniques, including sedimentation assay, electron microscopy (EM), and ThS fluorescence and LS analyses, have been employed. Concerning the LS method which measures the turbidity of the reaction solution, the 90° LS approach using laser light as the incident light has proven to be useful for monitoring tau aggregation under physiological conditions (around 4 μM) (*20*). However, for the first time, we succeeded in monitoring the aggregation process of tau repeat peptides using the conventional light used for fluorescence measurement. By carefully selecting the wavelength of the incident light, it was possible to improve the LS sensitivity in monitoring the aggregation process of the repeat peptides. Compared with the LLS method, this method can be performed directly on the instrument used for ThS fluorescence measurement, which is another approach to monitoring the *in vitro* aggregation of the tau protein, thus making the observation of two different filament formation behaviors on the same instrument possible.

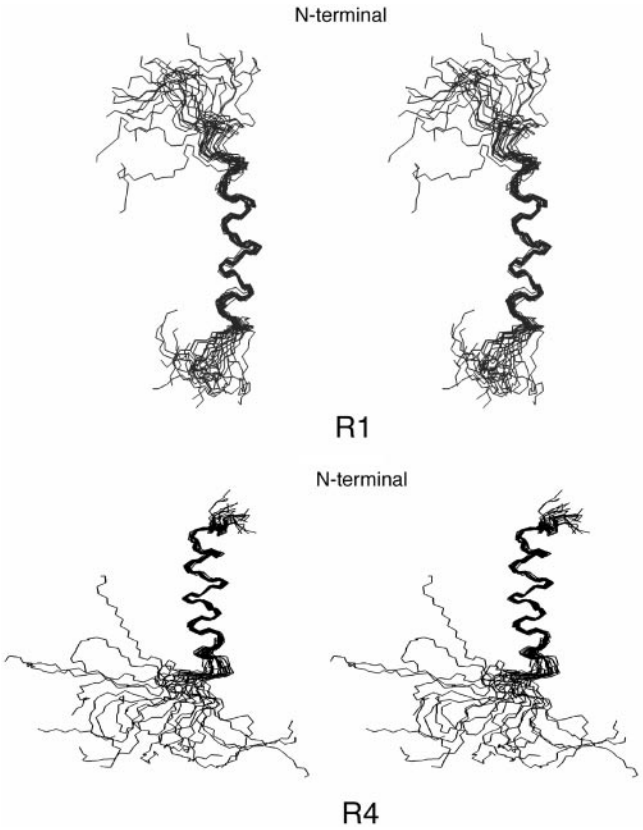

Fig. 10. **Stereoscopic superpositions of the most stable 20 conformers of R1 and R4.** Each conformer is projected so as to be superimposed on the Leu10–Lys24 (R1) or Ser5–Ser20 (R4) sequence. The upper and lower sides of conformers correspond to the N- and C-terminal regions, respectively.

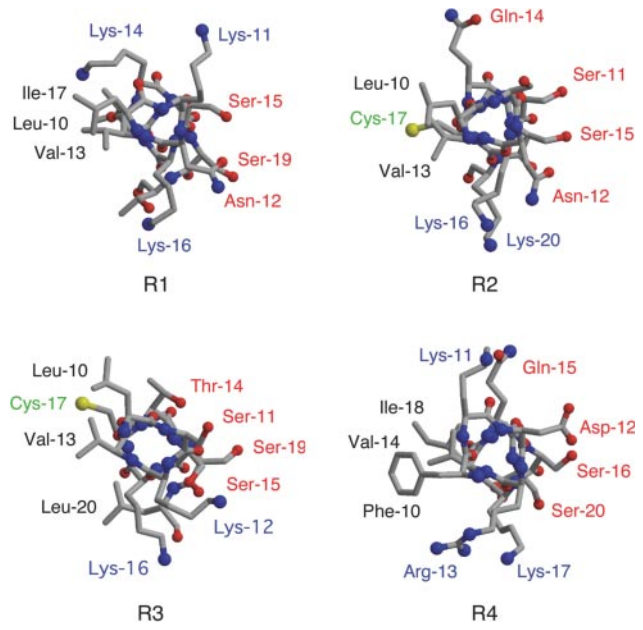

Fig. 11. **Helical wheel drawings of 10–20 sequences of the most stable conformers of R1–R4, viewed from the N-terminal side.** Blue-, red- and black-colored letters represent basic, polar and hydrophobic residues, respectively. The cysteine residues in R2 and R3 are shown by green-colored letters.

The time–LS intensity profiles shown in Fig. 3 clarified the dynamic features of filament growth of each repeat peptide at a fixed concentration. On the other hand, the concentration–LS intensity profiles of the peptide filaments prepared by overnight reaction (Fig. 4) indicated the minimum concentration necessary to start the filament extension process, and reflect the ease of filament formation and the thermodynamic features of filament growth of each peptide.

Based on the concentration–LS intensity relationship of each repeat peptide (Fig. 5), the following discussion is possible: Among the four repeat peptides, the R3 peptide has the highest potency for starting the filament formation reaction because of its lowest critical concentration. The R1 and R4 peptides showed no marked filament formation under the present experimental conditions, probably in part due to the lack of intermolecular disulfide bond formation *via* their cysteine residues, as judged from the fact that a reducing agent such as DTT decreases the filament formations of R2, R3 and 4RMBD (*11*, *16*) significantly. The critical concentration of 3RMBD was significantly higher than that of R3. As 3RMBD is constructed by attaching R1 and R4 to the N- and C-terminal ends of the R3 peptide, respectively, this suggests that the R1 and R4 repeats in 3RMBD exert a negative effect on the R3-driven self-aggregation of 3RMBD. On the other hand, the critical concentration of 4RMBD was lower than that of 3RMBD, indicating the positive synergistic effect of the R2 repeat structure for the 4RMBD filament. The present data also suggest that the four repeat tau isoform (4RMBD) has a greater tendency to form filaments than the three repeat tau isoform (3RMBD). This would explain why four-repeat tau isoforms promote their PHF assembly faster than three-repeat isoforms (*30*). Since the shortest three-repeat isoform is expressed only in immature human brain (*31*), this result may also explain why the aged population has a higher risk of AD.

Another important parameter is the slope of the concentration–LS intensity curve in Fig. 4. Generally, the slope reveals the positive effect of the peptide concentration on filament formation. However, it should be noted that the slope of the concentration–LS intensity curve is different. In addition to the positive effect of peptide concentration on the filament extension process, the slope is affected by many factors, for example, the morphology of the filament formed by different tau constructs. Although the intensity of light scattering is mainly dependent on the number of "scattering particles" in solution, the shape of the filament could also have some effect on light scattering. Any asymmetry from sphere shape will result in errors in the "Rayleigh Scattering" theory. For filaments formed at a certain concentration, the larger the size, the fewer the number. Therefore, if the tau constructs form very long filaments, the number will be fewer and the slope of the concentration dependence curve will be smaller.

Previously, we reported the EM images of the R2, R3 and 4RMBD filaments (*11*, *16*) prepared in the same manner as those in Fig. 4. Both the R2 and R3 peptides produced nonphysiological filaments without helical structures. In contrast, the EM image of 4RMBD shows a typical paired-helical filament structure similar to that

of full-length tau protein (*11*), in which the double-stranded twisted appearance is formed with a crossover repeat of ~80 nm. Similar PHF formations have been reported for 3RMBD (*8*). This implies that the collaborative aggregation of the R1 and R4 repeat units is necessary for the intact PHF formation of tau MBD, despite their weak abilities to self-assemble.

On the other hand, the profiles shown in Fig. 6 suggest that the filament formation of R3 is mainly dominated by the extension process (nucleation rate > extension rate), whereas the filament formation of the R2 peptide is dominated by the nucleation process (extension rate ⩾ nucleation rate). The EM images of the R2 and R3 peptides (*11*, *16*) support this interpretation, because it is reasonable to consider that the long and wide filaments of R2 are mainly formed *via* the fast extension/slow nucleation process, whereas the short and narrow filaments of R3 are result from the fast nucleation/slow extension process. This is also supported by the seed experiment (Fig. 7), in which the R2 seeds promoted the assembly of the R2 peptide according to a first-order reaction. Since the filaments of the R3 peptide are mainly formed by self-aggregation *via* the fast nucleation reaction and minimally affected by any type of seed (*16*), the contributions of the R2 and R3 peptides to the MBD filament formation process are obviously different.

To clarify which structural part in the tau MBD region is the most flexible and solvent-sensitive, we investigated the TFE-induced conformational change of each repeat peptide by CD and NMR spectroscopic methods. The CD spectral comparison of R1–R4 showed TFE-induced transition degrees of R1 ≈ R2 ≈ R4 > R3 from a random structure to an α-helical structure in aqueous solution, and the conformational comparison of R1–R4 in TFE solution (Fig. 12) clarified that the R3 peptide takes an amphipathic extended structure and an α-helical structure at the N-terminal Val1–Lys6 and central Leu10–Leu20 regions, respectively; on the other hand, the averaged backbone conformations of the R1, R2 and R4 peptides consist of a sequential mixture of amphipathic α-helical and random structures. The N-terminal Val1–Lys6 extended structure of R3 has been reported to be rigid even in aqueous solution (*15*), and to play an important role in the PHF formation of the tau protein (*32*), together with the Lys12–Leu20 region (*33*). Thus, the fast nucleation-driven filament formation behavior of the R3 peptide should be closely related to this conformational feature. On the other hand, the conformational analyses of the repeat peptides suggested the importance of intermolecular disulfide bond formation for effective filament formation of tau MBD, as is supposed from the distribution of Cys residues in the helical wheel drawings of the R2 and R3 peptides (Fig. 11).

Generally, the filament formation by the tau protein can be divided into the following steps: activation → nucleation → extension → PHF formation (Fig. 2). Herein we discuss the possible structural/functional role of each repeat unit in the initial *in vitro* filament formation process of 4RMBD, on the basis of the above results concerning the conformational, associational and morphological features of four repeat peptides (R1–R4). A dimer formation

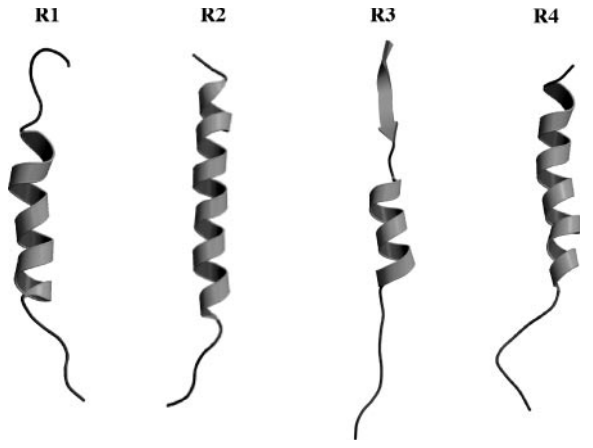

Fig. 12. **Averaged backbone conformations of R1–R4 peptides in TFE solution, constructed by ^{1}H-NMR and molecular modeling analyses. The N- and C-terminal regions correspond to the upper and lower sides, respectively**. The arrow, ribbon and thin line represent the β-sheet, α-helical and random structures, respectively.

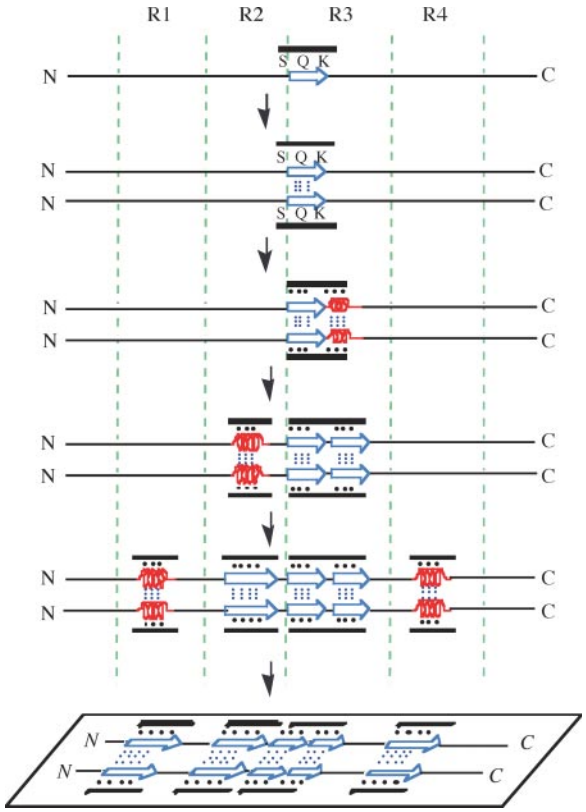

Fig. 13. **A model for the in vitro repeat structure-dependent dimer formation of 4RMBD**. Dimer formation of 4RMBD is promoted by a polyanion such as heparin. The polyanion promotes (a) hydrophobic interactions between the R3 extended regions through electrostatic interactions of the polyanion with the polar S, Q and K residues of the amphipathic extended region, and (b) the successive hydrophobic interactions between amphipathic the α-helical–like intermediate structures of the R1–R4 peptides through electrostatic interactions of the polyanion with the polar and/or basic residues of the polyanion-induced amphipathic intermediate structures of repeat peptides. In this figure, the black bars, blue open arrows and red springs represent polyanions, β-sheet structures, and α-helical–like intermediate structures, respectively. The large and small dotted lines represent electrostatic (including hydrogen bonds) and hydrophobic interactions, respectively. N and C indicate the N- and C-terminals of 4RMBD, respectively.

model of 4RMBD is proposed in Fig. 13, which could be a unit structure for PHF formation. Since it has recently been shown by Mizushima *et al*. (unpublished results) that heparin promotes the transformation of the random conformations of the R1 to R4 repeat peptides in water to β-sheet structures *via* helical-like intermediate structures, the proposed model is based on the repeat peptide being readily induced to take an amphipathic extended- or helical-like structure through the electrostatic interactions with heparin, because the peptide has been shown to be flexible and to have a high tendency of adopting an amphipathic conformation. The R3 repeat is the most likely region to act a trigger to start the molecular aggregation of 4RMBD, because it shows the fastest self-aggregation behavior among the four repeat peptides. The N-terminal Val1–Lys6 region of R3 would take an amphipathic extended structure in which the polar S, Q and K residues located on the same hydrophilic side form electrostatic interactions with the acidic groups of heparin (the 1st step in Fig. 13), and associate with the facing R3 extended region through hydrophobic interactions (the 2nd step). Similarly, the Leu10–Leu20 region of R3 would also be induced to adopt an amphipathic α-helical–like intermediate structure through electrostatic interactions with anionic heparin, leading to an association through the hydrophobic interactions between the amphipathic structures (the 3rd step). These two factors would be an important driving force for the formation of a parallel dimer structure of 4RMBDs induced by heparin, in which an intermolecular disulfide bond formation between two neighboring Cys residues located on the hydrophobic side of the amphipathic structure stabilizes the dimer structure; increased PHF formation through intermolecular disulfide bonds between MBDs has been reported (*34*). On the other hand, the amphipathic helical-like intermediate structures of two neighboring R2 repeats, induced by electrostatic interaction with heparin and intermolecular disulfide bond formation, would associate positively with each other through hydrophobic interactions and then stabilize the dimer structure of 4RMBD (the 4th step). The heparin-induced amphipathic helical-like orientations of R1 and R4 would also contribute to the stabilization of the 4RMBD parallel dimer structure through hydrophobic interactions (the 5th step); the hydrophobic interactions between two neighboring R1/R4 amphipathic structures would be insufficient to stabilize the dimer structure and rather exert a negative effect on the R3-driven aggregation of 3RMBD. Since the heparin-induced transition of 4RMBD from its monomeric random structure to a β-sheet-like dimeric structure in buffer solution (pH 7.6) is suggested by the CD spectral, dynamic LS and gel-filtration measurements (*11*), we believe that this proposed parallel dimer consisting of a planar sheet structure could behave as a unit structure for PHF formation. After the formation of this dimeric structures, they would associate with one another in an antiparallel fashion and expand perpendicular to this planar unit structure, thus forming the cross β-structure of PHF (fibril). Many assembly models of the tau protein have been proposed. However, to our knowledge, the possible contribution of each repeat structure to PHF formation of tau MBD has not yet been reported. Therefore, we believe that the present results are useful when considering the repeat structure-dependent step-by-step PHF formation mechanism of tau protein.

This work was supported by The Science Research Promotion Fund of The Promotion and Mutual Aid Corporation for Private Schools of Japan, and by Grants-in-Aid for Scientific Research from the Ministry of Education, Culture, Sports, Science and Technology of Japan. T.-M.Y. also thanks the National Natural Science Foundation of China (20472065), and a Postdoctoral Fellowship for Foreign Researchers from JSPS for financial support.

REFERENCES

1. Goedert, M., Jakes, R., Spillantini, M.G., and Crowther, R.A. (1994) In *Microtubules* (Hyams, J. and Lloyd, C. eds.) pp. 183–200, Wiley-Liss, New York
2. Goedert, M. and Spillantini, M.G. (2000) Tau mutations in frontotemporal dementia FTDP-17 and their relevance for Alzheimer's disease. *Biochim. Biophys. Acta* **1502**, 110–121
3. Goedert, M., Wischik, C.M., Crowther, R.A., Walker, J.E., and Klug, A. (1988) Cloning and sequencing of the cDNA encoding a core protein of the paired helical filament of Alzheimer's disease: identification as the microtubule-associated protein tau. *Proc. Natl. Acad. Sci. USA* **85**, 4051–4055
4. Lee, G., Cowan, N., and Kirschner, M. (1988) The primary structure and heterogeneity of tau protein from mouse brain. *Science* **239**, 285–288
5. Goedert, M., Spillantini, M.G., Jakes, R., Rutherford, D., and Crowther, R.A. (1989) Multiple isoforms of human microtubule-associated protein tau: sequences and localization in neurofibrillary tangles of Alzheimer's disease. *Neuron* **3**, 519–526
6. Friedhoff, F., Von Bergen, M., Mandelkow, E.-M., and Mandelkow, E. (1998) A nucleated assembly mechanism of Alzheimer paired helical filaments. *Proc. Natl. Acad. Sci. USA* **95**, 15712–15717
7. Wille, H., Drewes, G., Biernat, J., Mandelkow, E.-M. and Mandelkow, E. (1992) Alzheimer-like paired helical filaments and antiparallel dimers formed from microtubule-associated protein tau *in vitro*. *J. Cell. Biol.* **118**, 573–584
8. Barghorn, S. and Mandelkow, E. (2002) Toward a unified scheme for the aggregation of tau into Alzheimer paired helical filament. *Biochemistry* **41**, 14885–14896
9. Gamblin, T.C., Berry, R.W., and Binder, L.I. (2003) Modeling tau polymerization in vitro: a review and synthesis. *Biochemistry* **42**, 15009–15017
10. Barghorn, S., Davies, P., and Mandelkow, E. (2004) Tau paired helical filaments from Alzheimer's disease brain and assembled in vitro are based on β–structure in the core domain. *Biochemistry* **43**, 1694–1703
11. Yao, T. –M., Tomoo, K., Ishida, T., Hasegawa, H., Sasaki, M., and Taniguchi, T. (2003) Aggregation analysis of the microtubule-binding domain in tau protein by spectroscopic methods. *J. Biochem.* **134**, 91–99
12. Perez, M., Valpuesta, J.M., Medina, M., Montejo de Garcini, E., and Avila, J. (1996) Polymerization of τ into filament in the presence of heparin: the minimal sequence required for τ–τ interaction. *J. Neurochem.* **67**, 1183–1190
13. Spillantini, M.G., Murrell, J.R., Goedert, M., Farlow, M.R., Klug, A., and Ghetti, B. (1998) Mutation in the tau gene in familial multiple system tauopathy with presenile dementia. *Proc. Natl. Acad. Sci. USA* **95**, 7737–7741
14. Minoura, K., Tomoo, K., Ishida, T., Hasegawa, H., Sasaki, M., and Taniguchi, T. (2002) Amphipathic helical behaviour of the third repeat fragment in the tau microtubule-binding domain, studied by ^{1}H NMR spectroscopy. *Biochem. Biophys. Res. Commun.* **294**, 210–214

15. Minoura, K., Tomoo, K., Ishida, T., Hasegawa, H., Sasaki, M., and Taniguchi, T. (2003) Solvent-dependent conformation of the third repeat fragment in the microtubule-binding domain of tau protein, analyzed by ^{1}H-NMR spectroscopy and molecular modeling calculation. *Bull. Chem. Soc. Jpn.* **76**, 1617–1624
16. Minoura, K., Yao, T. –M., Tomoo, K., Sumida, M., Sasaki, M., Taniguchi, T., and Ishida, T. (2004) Differential associational and conformational behaviours between the second and third repeat fragments in the tau microtubule-binding domain. *Eur. J. Biochem.* **271**, 545–552
17. Hiraoka, S., Yao, T. –M., Minoura, K., Tomoo, K., Sumida, M., Taniguchi, T., and Ishida, T. (2004) Conformational transition state is responsible for assembly of microtubule-binding domain of tau protein. *Biochem. Biophys. Res. Commun.* **315**, 659–663
18. Minoura, K., Mizushima, F., Tokimasa, M., Hiraoka, S., Tomoo, K., Sumida, M., Taniguchi, T., and Ishida, T. (2005) Structural evaluation of conformational transition state responsible for self-assembly of tau microtubule-binding domain. *Biochem. Biophys. Res. Commun.* **327**, 1100–1104
19. Lomakin, A., Benedek, G.B., and Teplow, D.B. (1999) Monitoring protein assembly using aquaelastic light scattering spectroscopy. *Methods Enzymol.* **309**, 429–459
20. Gamblin, T.C., King, M.E., Dawson, H., Vitek, M.P., Kuret, J., Berry, R.W., and Binder, L.I. (2000) *In vitro* polymerization of tau protein monitored by laser light scattering: method and application to the study of FTDP-17 mutants. *Biochemistry* **39**, 6136–6144
21. Friedhoff, P., Schneider, A.E.M., Davies, P., and Mandelkow, E. (1998) Rapid assembly of Alzheimer-like paired helical filaments from microtubule-associated protein tau monitored by fluorescence in solution. *Biochemistry* **37**, 10223–10230
22. Jarrett, J.T. and Lansbury, P.T. (1993) Seeding "one-dimensional crystallization" of amyloid: a pathogenic mechanism in Alzheimer's disease and scrapie? *Cell* **73**, 1055–1058
23. Krebs, M.R.H., Bromley, E.H.C., and Donald, A.M. (2005) The binding of thioflavin-T to amyloid fibrils: localisation and implications. *J. Struct. Biol.* **149**, 30–37
24. Bystrov, V.F. (1976) Spin-spin coupling and the conformational states of peptide systems. *Prog. Nucl. Magn. Reson. Spectrosc.* **10**, 41–81
25. Nilges, M., Clore, G.M., and Gronenborn, A.M. (1988) Determination of three-dimensional structures of proteins from interproton distance data by hybrid distance geometry-dynamical simulated annealing calculations. *FEBS Lett.* **229**, 317–324
26. Brunger, A.T., Adams, P.D., Clore, G.M., DeLano, W.L., Gros, P., Grosse-Kunstleve, R.W., Jiang, J.S., Kuszewski, J., Nilges, M., Pannu, N.S., Read, R.J., Rice, L.M., Simonson, T., and Warren, G.L. (1998) Crystallography and NMR system: a new software suited for macromolecular structure determination. *Acta Crystallogr.* **D54**, 905–921
27. Koradi, R., Billeter, M., and Wuthrich, K. (1996) MOLMOL: a program for display and analysis of macromolecular structures. *J. Mol. Graphics* **14**, 51–55
28. Van Holde, K.E. (1971) *Physical Biochemistry*, Prentice-Hall, Englewood Cliffs, NJ
29. Chen, Y.H., Yang, J.T., and Martinez, H.M. (1972) Determination of the secondary structures of proteins by circular dichroism and optical rotatory dispersion. *Biochemistry* **11**, 4120–4131
30. Goedert, M. and Jakes, R. (1990) Expression of separate isoforms of human tau protein: correlation with the tau pattern in brain and effects on tubulin polymerization. *EMBO J.* **9**, 4225–4230
31. Goedert, M., Spillantini, M.G., Potier, M.C., Ulrich, J., and Crowther, R.A. (1989) Cloning and sequencing of the cDNA encoding an isoform of microtubule-associated protein tau containing four tandem repeats: differential expression of tau protein mRNAs in human brain. *EMBO J.* **8**, 393–399
32. Von Bergen, M., Friedhoff, P., Biernat, J., Heberle, J., Mandelkow, E.M., and Mandelkow, E. (2000) Assembly of tau protein into Alzheimer paired helical filaments depends on a local sequence motif ((306)VQIVYK(311)) forming beta structure. *Proc. Natl. Acad. Sci. USA* **97**, 5129–5134
33. Perez, M., Arrasate, M., Montejo de Garcini, E., Munoz, V., and Avila, J. (2001) In vitro assembly of tau protein: mapping the regions involved in filament formation. *Biochemistry* **40**, 5983–5991
34. Bhattacharya, K., Rank, K.B., Evans, D.B., and Sharma, S.K. (2001) Role of cysteine-291 and cysteine-322 in the polymerization of human tau into Alzheimer-like filaments. *Biochem. Biophys. Res. Commun.* **285**, 20–26